Draft version September 27, 2019
Typeset using LaTeX **twocolumn** style in AASTeX63

The Physical Origins of the Identified and Still Missing Components of the Warm-Hot Intergalactic Medium: Insights from Deep Surveys in the Field of Blazar 1ES1553+113

Sean D. Johnson,[1,2,*] John S. Mulchaey,[2] Hsiao-Wen Chen,[3] Nastasha A. Wijers,[4] Thomas Connor,[2] Sowgat Muzahid,[4] Joop Schaye,[4] Renyue Cen,[1] Scott G. Carlsten,[1] Jane Charlton,[5] Maria R. Drout,[6,2] Andy D. Goulding,[1] Terese T. Hansen,[7] Gregory L. Walth,[2]

[1]*Department of Astrophysical Sciences, 4 Ivy Lane, Princeton University, Princeton, NJ 08544, USA*
[2]*The Observatories of the Carnegie Institution for Science, 813 Santa Barbara Street, Pasadena, CA 91101, USA*
[3]*Department of Astronomy & Astrophysics, The University of Chicago, 5640 S. Ellis Avenue, Chicago, IL 60637, USA*
[4]*Leiden Observatory, Leiden University, PO Box 9513, NL-2300 RA Leiden, the Netherlands*
[5]*Dept. of Astronomy & Astrophysics, The Pennsylvania State University, 525 Davey Lab, University Park, PA 16802, USA*
[6]*Department of Astronomy and Astrophysics, University of Toronto, 50 St. George Street, Toronto, Ontario, M5S, 3H4 Canada*
[7]*Mitchell Institute for Fundamental Physics and Astronomy and Department of Physics and Astronomy, Texas A&M University, College Station, TX 77843-4242, USA*

(Received XX XX, 2019; Revised XX XX, 2019; Accepted XX)

Submitted to ApJL

ABSTRACT

The relationship between galaxies and the state/chemical enrichment of the warm-hot intergalactic medium (WHIM) expected to dominate the baryon budget at low-z provides sensitive constraints on structure formation and galaxy evolution models. We present a deep redshift survey in the field of 1ES1553+113, a blazar with a unique combination of UV+X-ray spectra for surveys of the circum-/intergalactic medium (CGM/IGM). Nicastro et al. (2018) reported the detection of two O VII WHIM absorbers at $z = 0.4339$ and 0.3551 in its spectrum, suggesting that the WHIM is metal-rich and sufficient to close the missing baryons problem. Our survey indicates that the blazar is a member of a $z = 0.433$ group and that the higher-z O VII candidate arises from its intragroup medium. The resulting bias precludes its use in baryon censuses. The $z = 0.3551$ candidate occurs in an isolated environment 630 kpc from the nearest galaxy (with stellar mass $\log M_*/M_\odot \approx 9.7$) which we show is unexpected for the WHIM. Finally, we characterize the galactic environments of broad H I Lyα absorbers (Doppler widths of $b = 40 - 80$ km s^{-1}; $T \lesssim 4 \times 10^5$ K) which provide metallicity independent WHIM probes. On average, broad Lyα absorbers are $\approx$2$\times$ closer to the nearest luminous ($L > 0.25L_*$) galaxy (700 kpc) than narrow ($b < 30$ km s^{-1}; $T \lesssim 4 \times 10^5$ K) ones (1300 kpc) but $\approx$2$\times$ further than O VI absorbers (350 kpc). These observations suggest that gravitational collapse heats portions of the IGM to form the WHIM but with feedback that does not enrich the IGM far beyond galaxy/group halos to levels currently observable in UV/X-ray metal lines.

Keywords: intergalactic medium – quasars: absorption lines – BL Lacertae objects: 1ES 1553+113

1. INTRODUCTION

Cosmological simulations predict that gravitational shocks associated with structure formation will heat a large fraction of the cool ($T \approx 10^4$ K) intergalactic medium (IGM) that dominates the baryon budget in the early Universe to form a Warm-Hot Intergalactic Medium (WHIM; $T \approx 10^5 - 10^7$ K) at $z \lesssim 1$ (e.g. Cen & Ostriker 1999). The predicted physical state and enrichment levels of the WHIM depend sensitively on stellar and black hole feedback which provide additional heating and chemical enrichment (e.g. Rahmati et al. 2016; Nelson et al. 2018; Wijers et al. 2019). Observations of the WHIM and its relationship to galaxies can, therefore, serve as a check of our cosmological paradigm and as a laboratory for studying galaxy evolution.

While observationally elusive, the WHIM can be detected via absorption spectroscopy through ionic transitions in the UV and X-ray as well as through metallicity independent probes such as broad H I Lyα absorption

Corresponding author: Sean D. Johnson
sdj@astro.princeton.edu

* Hubble & Carnegie-Princeton fellow

(e.g. Danforth et al. 2010), the Sunyaev-Zel'dovich (SZ) effect (e.g. de Graaff et al. 2019), and the dispersion measure of fast radio bursts (FRBs; e.g. Bannister et al. 2019; Ravi et al. 2019). Surveys of the highly ionized phases of the CGM/IGM traced by O VI (e.g. Danforth et al. 2016), Ne VIII (e.g. Pachat et al. 2017; Frank et al. 2018), and Mg X (Qu & Bregman 2016) with the Cosmic Origins Spectrograph (Green et al. 2012) on the *Hubble Space Telescope* (HST) can account for a large fraction of the baryons expected in the WHIM but leave $\sim 30\%$ missing (e.g. Shull et al. 2012) and potentially in a chemically pristine or more highly ionized phase.

Surveys of CGM/IGM around galaxies find that metal ion absorption is common in the CGM at projected distances (d) less than the estimated galaxy host halo virial radii ($R_{\rm h}$) but comparatively rare at larger distances (e.g. Liang & Chen 2014; Turner et al. 2014; Johnson et al. 2015, 2017; Burchett et al. 2019). These observations suggest that feedback may be ineffective at enriching the IGM far beyond galaxy halos. Indeed, the statistical detection of SZ signal from the filaments between massive galaxies (de Graaff et al. 2019) can potentially account for the remaining missing baryons, suggesting that a substantial portion of the WHIM exhibits low metallicities ($< \frac{1}{10}$ solar; Liang & Chen 2014; Johnson et al. 2015) or high temperatures ($T > 6 \times 10^5$ K) not traced in the UV.

New insights into chemical enrichment mechanisms and the physical state of the CGM/IGM require deep galaxy surveys in fields with UV and X-ray absorption spectra. Blazars are ideal for such studies because of their high UV/X-ray flux levels. Recently, Nicastro et al. (2018) obtained a 1.7 Msec *XMM-Newton* X-ray spectrum of the blazar 1ES 1553+113, reaching the S/N levels required to detect hot CGM/IGM absorbers individually over a large redshift pathlength for the first time. The X-ray spectrum revealed two candidate O VII absorption systems at $z = 0.4339$ and 0.3551, each with statistical significance of $\approx 3-4\sigma$, though we note that systematic/non-Gaussian errors (e.g. Nevalainen et al. 2019) and contamination (e.g. Nicastro et al. 2016) have led to past controversies over X-ray absorbers. Nevertheless, taken together, the two O VII absorbers reported by Nicastro et al. (2018) suggest that the hot phase of the CGM/IGM is metal-rich and accounts for $10-70\%$ of the baryon budget. However, the combination of a poorly constrained blazar redshift (due to a featureless spectrum) and limited complementary galaxy surveys complicates the interpretation of absorbers toward 1ES 1553+113.

Here, we present a deep and highly complete galaxy redshift survey in the field of 1ES 1553+113. When combined with UV absorption spectra, the survey enables a precise measurement of the redshift of 1ES 1553+113 and provides insights into the origins of intervening IGM/CGM systems. The letter proceeds as follows: In Section 2, we describe the galaxy survey and UV spectroscopy. In Section 3, we combine these datasets to infer the blazar redshift. In Section 4, we characterize the galactic environments of the candidate WHIM absorbers and draw insights into their origins.

We adopt a flat Λ cosmology with $\Omega_{\rm m} = 0.3$, $\Omega_\Lambda = 0.7$, and $H_0 = 70\ {\rm km\,s^{-1}\,Mpc^{-1}}$. All magnitudes are in the AB system. We define the knee in the galaxy luminosity function, L_*, as $M_r = -21.5$ (Loveday et al. 2012).

2. OBSERVATIONS AND DATA

2.1. *Galaxy survey data*

To study the relationship between galaxies and the IGM, we conducted a deep and highly complete redshift survey targeting galaxies of $m_r < 23.5$ mag in the field of 1ES 1553+113 with multi-slit spectrographs on the Magellan Telescopes. We acquired deep g-, r-, and i-band images with MOSAIC on the Mayall telescope with 1800 sec of exposure in each filter under $1''$ seeing (PI: Johnson; PID: 2015A-0187) and an *HST* image with the ACS+F814W filter and 1200 sec of exposure (PI: Mulchaey; PID: 13024). We processed the data as described in Chen & Mulchaey (2009) and Johnson et al. (2015). In total, we measured spectroscopic redshifts for 921 galaxies at angular distances of $\Delta\theta < 14'$ from the blazar sightline and also include 25 redshifts from Prochaska et al. (2011) and one from Keeney et al. (2018). Redshift histograms and completeness levels for galaxies of $L \gtrsim 0.25L_*$ ($> 90\%$ at projected distances of $d < 500$ kpc and $z < 0.5$) are shown in Figure 1.

The survey results are summarized in Table 1 which reports coordinates, apparent magnitudes (m_g, m_r, m_i), redshift quality ("g" for secure redshifts and "s" for single-line redshifts), redshift ($z_{\rm gal}$), rest-frame $M_g - M_r$ color, absolute rest-frame r-band magnitude (M_r), stellar mass ($\log M_*/M_\odot$), and projected angular & physical separations from the blazar sightline ($\Delta\theta$ & d). The absolute magnitudes include k-corrections, and the stellar masses are estimated as in Johnson et al. (2015) assuming a Chabrier (2003) IMF. Typical uncertainties in the redshifts, magnitudes, and stellar masses are 60 ${\rm km\,s^{-1}}$, 0.1 mags, and 0.2 dex respectively. Table 1 is separated into sections by redshift within ± 1000 ${\rm km\,s^{-1}}$ of the two candidate O VII absorbers ($z = 0.4291 - 0.4387$; $0.3506 - 0.3596$), those at higher redshift ($z > 0.4387$), and all other redshifts. Figure 2 displays an image of the field with galaxy redshifts labeled.

2.2. *UV absorption spectroscopy*

The COS GTO team acquired G130M+G160M spectra of 1ES 1553+113 (PI: Green; PID: 11520, 12025) which are useful for inferring the redshift of the blazar based on the presence/absence of Lyα forest absorption. We retrieved all available COS spectra for 1ES 1553+113 from the *HST* archive and combined them into a single coadded spectrum as described in Johnson et al. (2013).

Table 1. Redshift survey summary with galaxies separated by redshift. The full table is available on the journal webpage.

R.A. (J2000)	Decl. (J2000)	m_g (AB)	m_r (AB)	m_i (AB)	quality	$z_{\rm gal}$ (AB)	$M_g - M_r$ (AB)	M_r	$\log M_*/M_\odot$	$\Delta\theta$ (arcsec)	d (pkpc)
$z_{\rm gal} > 0.4387$											
15:55:44.20	+11:11:04.6	23.1	22.1	21.4	g	0.5721	0.4	−21.3	10.3	26.1	170
15:55:43.91	+11:11:54.4	22.9	21.6	20.8	g	0.5963	0.5	−21.9	10.7	32.7	218
15:55:45.22	+11:11:20.7	23.3	21.9	21.1	g	0.6626	0.4	−22.2	10.6	32.3	226
15:55:45.38	+11:11:09.9	23.6	23.1	22.9	s	1.1130	0.2	−22.5	10.3	37.2	305
15:55:42.08	+11:10:32.1	23.1	22.2	22.0	g	0.5244	0.2	−20.2	9.4	54.1	338
15:55:44.62	+11:12:05.5	23.7	23.2	22.8	g	0.7753	0.2	−20.4	9.5	47.3	351
15:55:40.28	+11:10:55.3	23.9	23.1	22.3	g	0.8778	0.4	−21.9	10.5	49.9	386
15:55:47.24	+11:11:11.6	23.7	23.1	22.3	g	0.7270	0.2	−20.8	9.7	63.0	457
15:55:37.80	+11:11:43.4	23.0	21.4	20.9	g	0.4695	0.4	−21.2	10.3	79.5	469
15:55:38.87	+11:11:54.8	22.5	21.6	21.1	g	0.6935	0.2	−21.9	10.1	68.5	488
15:55:37.26	+11:11:23.9	23.2	21.5	20.9	g	0.4699	0.5	−21.3	10.5	85.2	503
⋮	⋮	⋮	⋮	⋮	⋮	⋮	⋮	⋮	⋮	⋮	
$z_{\rm gal} = 0.4291 - 0.4387$											
15:55:43.51	+11:11:13.0	23.9	22.7	22.5	g	0.4300	0.5	−20.8	10.2	13.2	74
15:55:43.19	+11:11:02.8	23.6	22.2	21.5	g	0.4347	0.6	−20.5	10.3	21.6	122
15:55:41.45	+11:11:29.1	25.4	23.3	22.9	s	0.4297	0.4	−19.1	9.5	23.9	134
15:55:42.76	+11:11:56.4	24.9	23.1	22.6	g	0.4344	0.7	−19.6	9.9	32.3	183
15:55:43.95	+11:11:56.7	21.4	19.6	18.9	g	0.4343	0.8	−23.2	11.4	35.0	198
15:55:42.94	+11:10:47.6	23.6	22.1	21.5	g	0.4329	0.6	−20.4	10.2	36.8	207
15:55:39.87	+11:11:46.8	24.3	23.3	23.4	g	0.4347	0.0	−18.5	8.7	51.9	293
15:55:46.15	+11:10:54.1	22.5	21.1	20.6	g	0.4328	0.5	−21.3	10.5	54.8	308
15:55:46.69	+11:11:07.7	23.1	22.3	22.2	g	0.4332	0.0	−19.5	9.1	56.1	316
15:55:47.25	+11:11:16.0	22.3	20.6	20.0	g	0.4328	0.7	−22.1	11.0	62.4	351
15:55:42.66	+11:12:29.8	23.4	22.1	21.9	g	0.4335	0.3	−20.0	9.6	65.7	370
15:55:42.53	+11:12:30.2	24.5	22.8	22.4	g	0.4339	0.5	−19.7	9.8	66.3	374
15:55:37.79	+11:10:51.4	24.3	23.0	22.8	g	0.4344	0.3	−19.2	9.3	84.0	474
15:55:44.56	+11:09:57.9	24.4	23.0	22.7	g	0.4327	0.4	−19.5	9.5	89.3	503
⋮	⋮	⋮	⋮	⋮	⋮	⋮	⋮	⋮	⋮	⋮	⋮
$z_{\rm gal} = 0.3506 - 0.3596$											
15:55:44.49	+11:09:19.3	22.8	21.7	21.4	g	0.3531	0.4	−19.9	9.7	126.8	630
15:56:02.12	+11:12:44.1	22.7	21.6	21.3	g	0.3537	0.4	−20.0	9.8	291.8	1451
15:55:29.10	+11:05:37.7	24.3	23.3	23.2	g	0.3547	0.1	−18.3	8.6	402.8	2007
15:55:47.81	+11:04:41.8	22.8	21.9	21.6	g	0.3596	0.4	−19.8	9.6	408.6	2054
15:55:41.14	+11:03:51.8	21.2	19.5	18.8	g	0.3580	0.8	−22.7	11.2	453.4	2273
15:56:13.90	+11:09:06.0	24.1	23.3	23.4	g	0.3590	0.0	−18.1	8.5	474.8	2384
15:55:24.61	+11:18:04.5	22.2	20.7	20.3	g	0.3538	0.6	−21.1	10.4	483.4	2405
15:55:12.93	+11:17:48.8	21.9	20.9	20.6	g	0.3542	0.4	−20.7	10.0	586.6	2920
15:55:52.15	+11:21:42.4	20.6	19.4	18.9	g	0.3531	0.6	−22.5	11.0	632.4	3142
⋮	⋮	⋮	⋮	⋮	⋮	⋮	⋮	⋮	⋮	⋮	⋮
Other redshifts											
15:55:07.77	+11:01:42.3	21.1	19.8	19.3	g	0.0017	1.2	−9.6	5.8	780.0	28
15:55:46.11	+11:11:49.4	23.5	22.9	22.8	g	0.1022	0.3	−15.6	7.8	51.6	97
15:55:44.01	+11:11:09.1	23.1	22.6	22.3	g	0.3892	0.3	−19.2	9.3	20.8	110
⋮	⋮	⋮	⋮	⋮	⋮	⋮	⋮	⋮	⋮	⋮	⋮

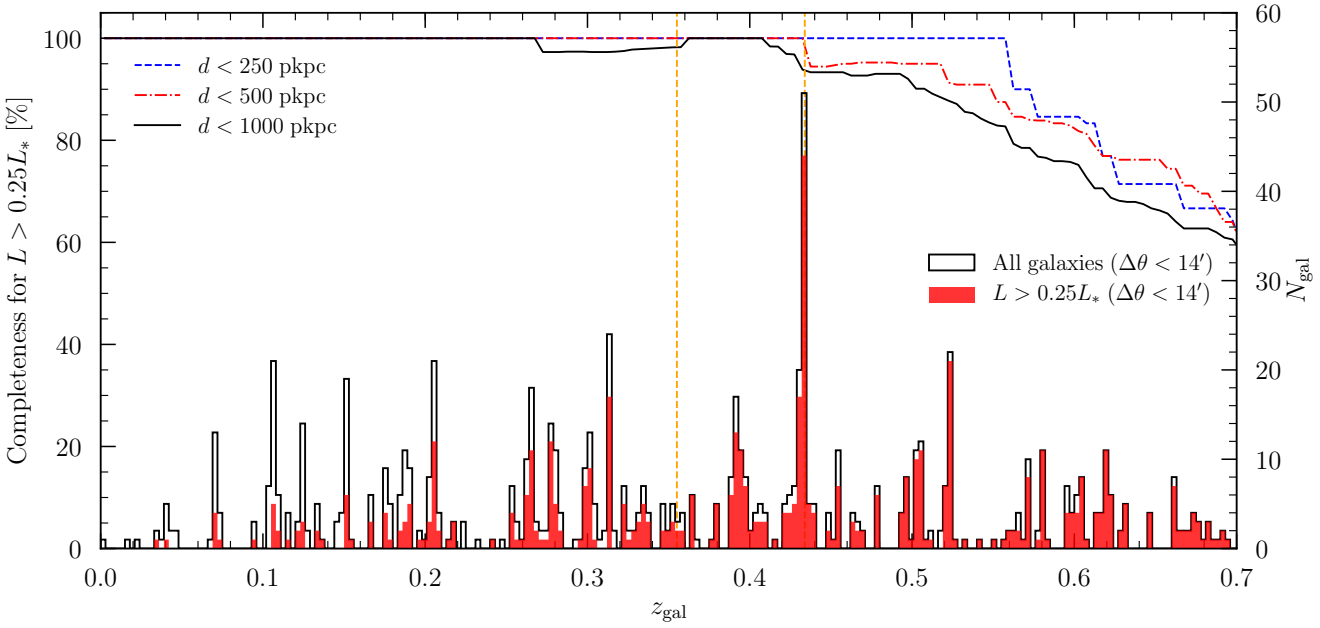

Figure 1. *Left axis*: Redshift completeness for galaxies of $L > 0.25L_*$ versus redshift at projected distances of $d < 250, 500$, and 1000 pkpc (top curves). *Right axis*: Redshift histograms with the full survey ($\Delta\theta < 14'$ from the blazar) in black and galaxies of $L > 0.25L_*$ in red. The redshifts of O VII candidates at $z = 0.3551$ and 0.4339 are shown in orange dashed lines.

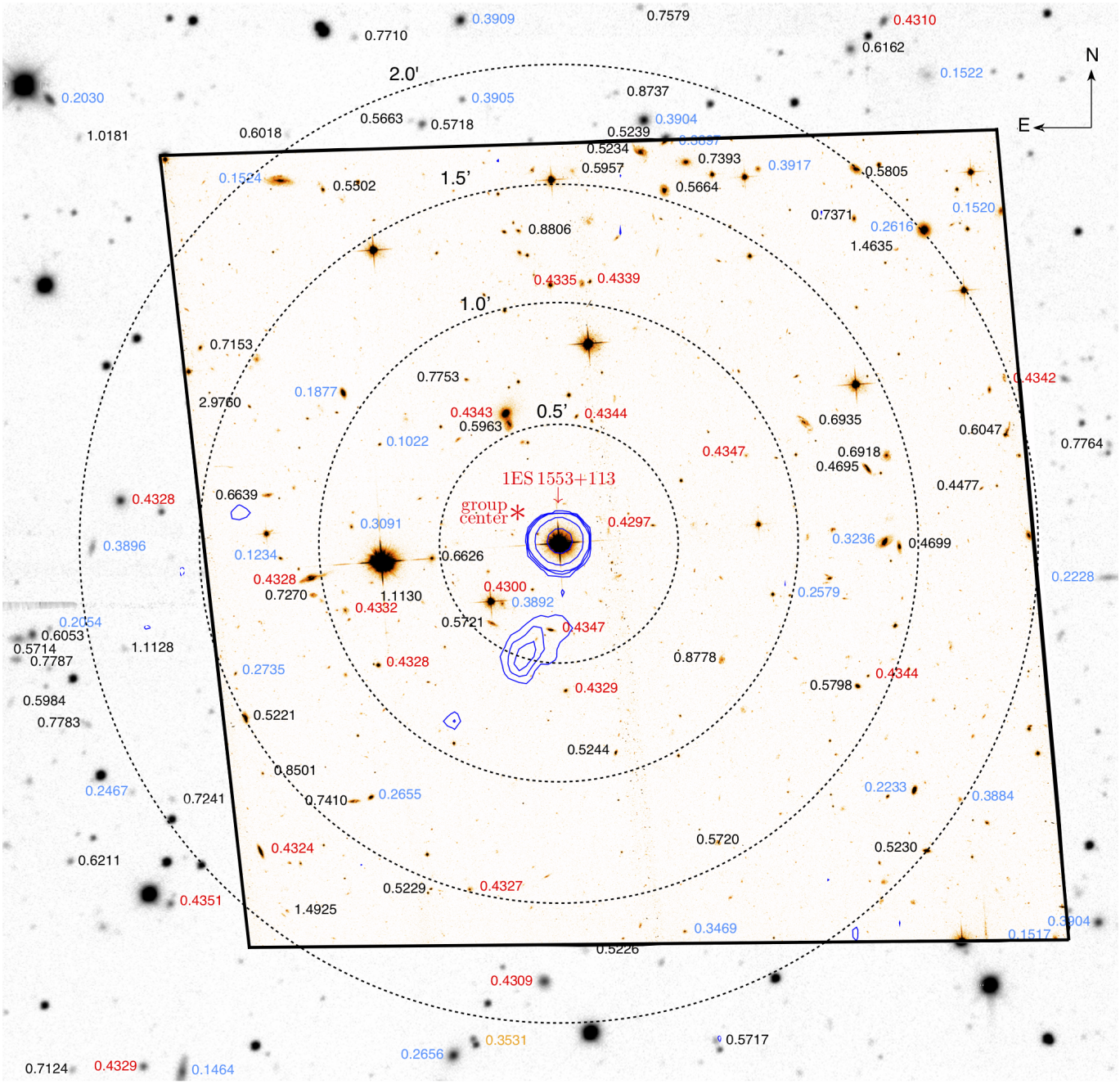

Figure 2. Image of the field of 1ES 1553+113 with galaxy redshifts labeled. The *HST* ACS+F814W image is shown in heat map while the outer regions not covered by the ACS are filled in with the MOSAIC i-band image shown in grey-scale. The galaxy labels are colored by redshift in black ($z > 0.4387$), red ($z = 0.4291 - 0.4387$), orange ($z = 0.3506 - 0.3596$), and blue (all other galaxies). The $z = 0.4291 - 0.4387$ and $z = 0.3506 - 0.3596$ redshift intervals correspond to ± 1000 km s^{-1} velocity intervals around the candidate O VII absorber redshifts. The blue contours from the FIRST (Becker et al. 1995) survey reveal a radio lobe. Dotted circles with radii of 0.5′, 1.0′, 1.5′, and 2.0′ are shown for scale (170, 340, 510, 680 pkpc at $z = 0.433$).

3. DISCOVERY AND REDSHIFT OF THE GROUP HOSTING 1ES 1553+113

Optical−X-ray spectra of 1ES 1553+113 exhibit no detected emission lines, preventing systemic redshift measurements (Landoni et al. 2014). The lack of a precise redshift measurement complicates the interpretation of absorption features in the spectrum of 1ES 1553+113 due to an inability to differentiate intervening IGM/CGM systems from associated absorption. Previous estimates of the redshift of 1ES 1553+113 based on the detection of intervening H I Lyα absorption (e.g. Danforth et al. 2010) and the shape of its γ-ray spectrum (e.g. Abramowski et al. 2015) imply $0.413 \lesssim z_{\rm sys} \lesssim 0.6$.

Blazars are typically hosted by luminous elliptical galaxies (e.g. Urry et al. 2000) in massive groups (e.g. Wurtz et al. 1997). Moreover, 1ES 1553+113 is a high energy peaked blazar which are thought to arise from beamed FR-I radio galaxies (e.g. Rector et al. 2000). 1ES 1553+113 exhibits a complex, one-sided radio-jet morphology (see Figure 2; Rector et al. 2003), indicating disturbance by a hot intragroup or intracluster medium. Identification of the blazar's host group therefore represents a precise means of inferring its redshift (e.g. Rovero et al. 2016; Farina et al. 2016).

To identify the host group of 1ES 1553+113, the top panel of Figure 3 displays the redshift histogram for galaxies of $L > 0.25L_*$ from our survey at $d < 500$ and < 1000 proper kpc (pkpc) from the blazar sightline. With high completeness levels of 100%, >90%, and >80% for galaxies of $L > 1.0, 0.5$, and $0.25\ L_*$ respectively at $d < 500$ pkpc and $z < 0.6$, our redshift survey is sensitive to galaxy groups over the full range of possible systemic redshifts for 1ES 1553+113. The only significant overdensity with multiple luminous galaxies near the blazar sightline is at $z \approx 0.433$, a strong indication that the blazar is a member of the $z = 0.433$ group.

The blazar host group consists of 7 (14) members of $L > 0.25L_*$ at $d < 500$ (1000) pkpc from the blazar and exhibits a light-weighted redshift of $z_{\rm group} = 0.433$. Not including the blazar host, the total stellar mass (luminosity) of the group is $\approx 8 \times 10^{11} M_\odot$ ($18\ L_*$) with $\approx 60\%$ (50%) coming from three massive, quiescent galaxies of $\log M_*/M_\odot > 11.0$. The measured line-of-sight velocity dispersion of the group is $\sigma_{\rm group} \approx 300$ km s^{-1}, which corresponds to an estimated dynamical mass of $M_{\rm dyn} \sim 2{-}5 \times 10^{13}\ M_\odot$. Such a massive group is consistent with expectations for the environment of blazars like 1ES 1553+113. Assuming that the luminosity of the blazar host galaxy is $L = 6L_*$ (Urry et al. 2000), the group light-weighted center is 13″ E. (70 pkpc) and 7″ N. (40 pkpc) of the blazar position.

The presence/absence of H I Lyα absorption in the blazar spectrum as a function of redshift can be used for an independent estimate of the blazar redshift. The archival COS spectrum of 1ES 1553+113 enables searches for H I Lyα absorption at $\lambda < 1796.7$ Å which corresponds to a maximum redshift of $z_{\rm Ly\alpha} = 0.478$. In this wavelength range, the S/N is sufficient to detect absorbers of $W_{\rm r} > 0.03$ Å at 3σ significance. The spectrum reveals 7 Lyα absorbers at $z = 0.350 - 0.413$ implying $z_{\rm sys} \gtrsim 0.413$ but none over the similar interval of $z = 0.413 - 0.478$ (bottom left panel of Figure 3).

To quantify the redshift constraint on 1ES 1553+113 from the Lyα forest with objects of similar luminosity, we identified 59 available QSOs with measured systemic redshifts, archival COS spectra, and IGM absorption line identifications from Danforth et al. (2016). For each QSO, we computed the difference between the systemic redshift and that of the highest redshift H I Lyα line with $W_r > 0.03$ Å in the spectrum, $\Delta z = z_{\rm sys} - \max(z_{\rm Ly\alpha})$. The resulting Δz distribution is shown in the bottom right panel of Figure 3. When combined with the highest redshift Lyα line in the spectrum of 1ES 1553+113 at $z = 0.413$ (50 pMpc from $z = 0.433$ where the UV background dominates), this distribution implies a 95% confidence interval for the redshift of 1ES 1553+113 of $z_{\rm sys} = 0.411 - 0.435$, consistent with membership of the $z = 0.433$ galaxy group. This constraint assumes that blazars and QSOs reside in similar intergalactic environments and is subject to small number statistics in the wings of the distribution. It will be further tested with new *HST* NUV spectra (PI: Muzahid, PID: 15835) for improved Lyα searches.

4. IMPLICATIONS FOR THE WHIM

4.1. *The origins of candidate WHIM X-ray absorbers*

Nicastro et al. (2018) identified two candidate WHIM O VII absorbers at $z = 0.4339$ and 0.3551 in the *XMM* spectrum of 1ES 1553+113, suggesting that the hot phase of the IGM is metal-rich and potentially closing the missing baryon problem. Neither O VII candidate is detected in O VI, O VIII, or lower ionization metal ions, similar to recent non-detections in an X-ray emitting cosmic filament (Connor et al. 2019). Here, we discuss the origins of these WHIM candidates based on our redshift survey.

As discussed in Section 3, 1ES 1553+113 is most likely a member of a galaxy group at $z = 0.433$. The identified O VII system at $z = 0.4339$ is therefore associated with the blazar environment and cannot be used in cosmic baryon censuses.

The blazar host group is part of a larger scale overdensity consisting of three additional groups at ≈ 1.5 pMpc S.E., ≈ 1.5 pMpc N.W., and ≈ 2.5 pMpc E.S.E. from the blazar. The O VII candidate could be due to WHIM from this overdensity, but photoionization from the blazar and UV background would be important. To evaluate the feasibility of the WHIM interpretation under these circumstances, we ran a series of Cloudy (Ferland et al. 2017) models to calculate the equilibrium O VI, O VII, and O VIII ion fractions as a function of distance from the blazar for gas with $n_{\rm H} = 10^{-5}{-}10^{-3}$ cm^{-3} and temperatures of $T = 10^5 - 10^7$ K including pho-

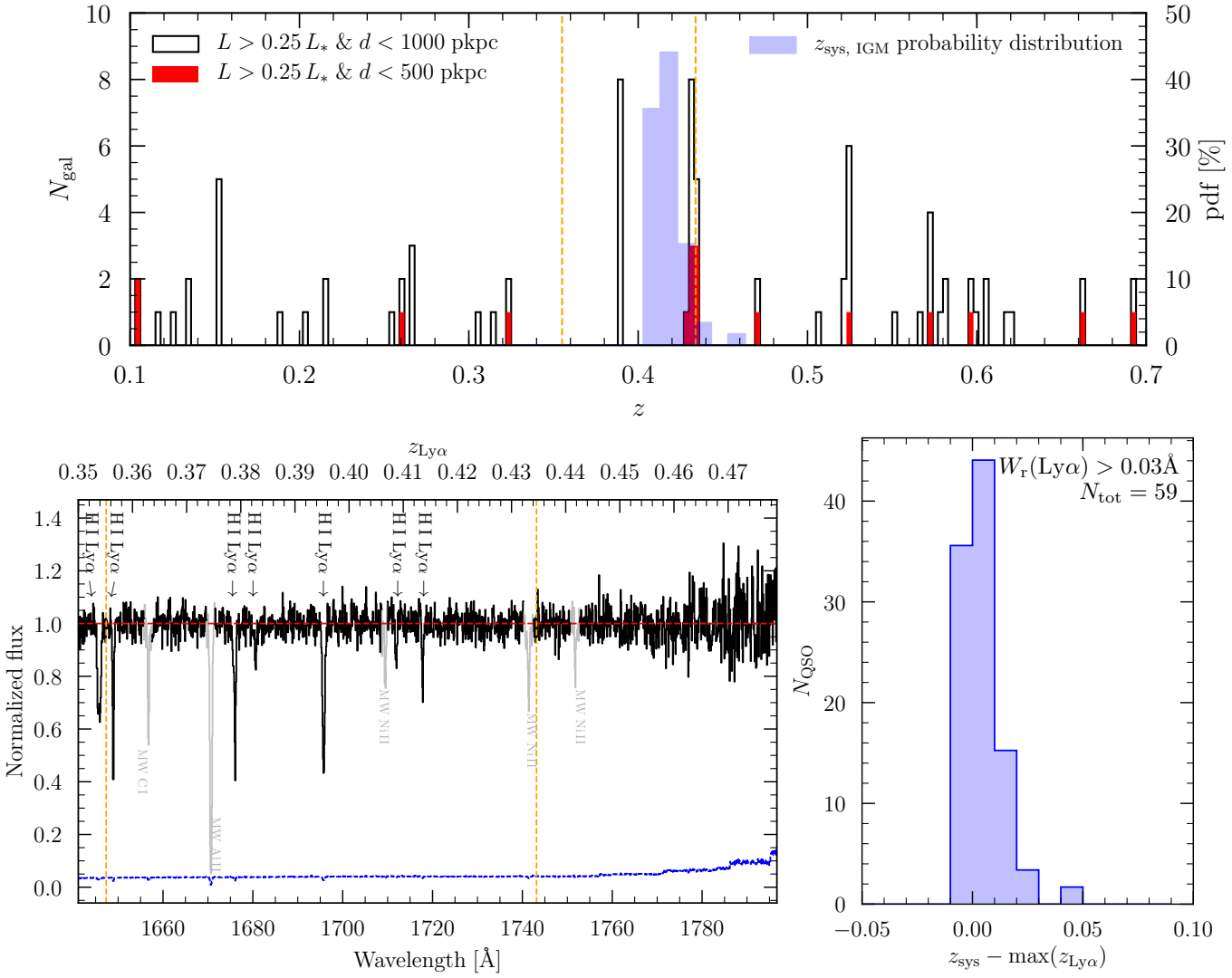

Figure 3. *Top*: Redshift histograms of galaxies with $L > 0.25L_*$ at $d < 1000$ (black histogram) and < 500 (red filled histogram) pkpc from the 1ES 1553+113 sightline. The only massive group in the field with multiple galaxies of $L > 0.25L_*$ near the blazar sightline is at $z = 0.433$, a strong indication that 1ES 1553+113 is a member of this galaxy group. *Bottom left*: Continuum normalized COS red-end spectrum of 1ES 1553+113 with flux in black and error in blue. Intervening H I Lyα absorption systems from the IGM are labeled, and Milky Way features are plotted in grey. The bottom axis shows the observed-frame wavelength while the top axis shows the corresponding Lyα redshift. Orange dashed lines mark the redshifts of the candidate O VII systems. *Bottom right*: Histogram of the redshift difference between QSO systemic redshifts and the highest redshift H I Lyα absorber of $W_{\rm r} > 0.03$ Å cataloged in COS spectra by Danforth et al. (2016), $z_{\rm sys} - \max(z_{\rm Ly\alpha})$. The resulting empirical constraint on the redshift of 1ES 1553+113 is shown in blue in the top panel (right axis).

toionization from the blazar ($\lambda L_\lambda = 10^{46}$ erg s^{-1} at 1 Rydberg and UV spectral slope of $\alpha = -1.4$ based the COS spectrum) and UV background (Khaire & Srianand 2019) as shown in Figure 4.

Nicastro et al. (2018) demonstrated that the O VII detection and O VI/O VIII non-detections at $z = 0.4339$ require a gas temperature of $T \approx 10^6$ K with little contribution from photoionization. This rules out WHIM gas with $n_{\rm H} < 10^{-4}$ cm^{-3} at any distance from the blazar because photoionization by the UV background is significant at such low densities (see Figure 4; Wijers et al. 2019). Denser hot gas of $n_{\rm H} = 10^{-4}$ (10^{-3}) cm^{-3} can reproduce the absorber properties but only at > 10 (1) pMpc from the blazar (see Figure 4). The $z = 0.4339$ O VII candidate is, therefore, unlikely to be due to low-density WHIM but may arise from hot CGM or intragroup medium (Mulchaey et al. 1996) in the blazar environment.

The $z = 0.3551$ O VII candidate resides in a comparatively isolated region with no galaxies at $d < 500$ pkpc from the sightline within $\Delta v = \pm 1000$ km s^{-1} from the absorber redshift despite 100% completeness levels

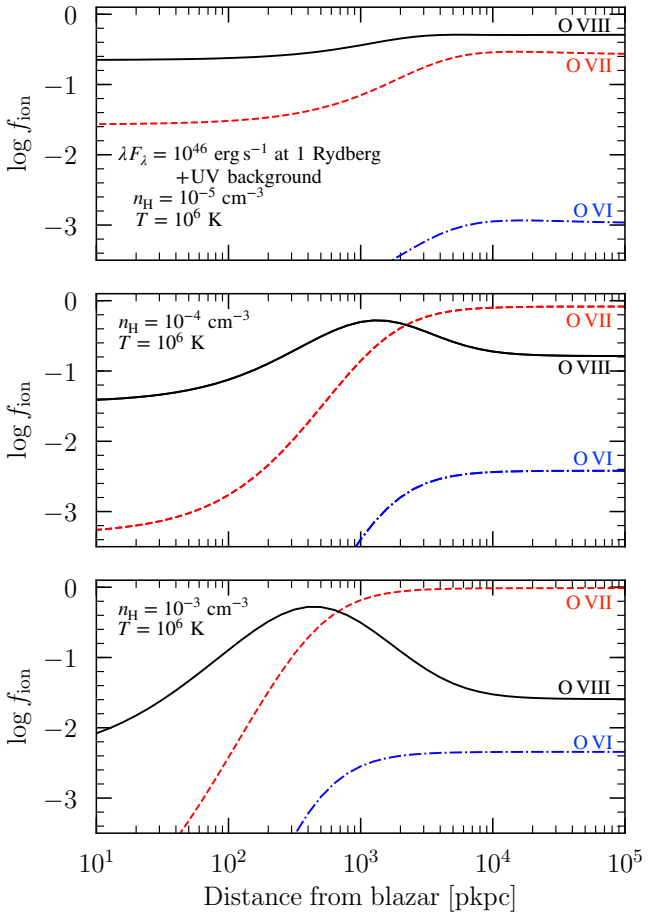

Figure 4. Metallicity independent equilibrium ion fraction of O VI (blue), O VII (red), and O VIII (black) as a function of distance from the blazar for gas with a temperature of $T = 10^6$ K and with a density of $n_H = 10^{-5}$ (top), 10^{-4} (middle), and 10^{-3} (bottom) cm^{-3}.

for galaxies of $L > 0.1L_*$. The nearest galaxy to the sightline is a star-forming galaxy of $\log M_*/M_\odot = 9.7$ at $z = 0.3531$ and $d = 630$ pkpc or $\approx 5\times$ its virial radius (estimated with the stellar-to-halo mass relation from Kravtsov et al. (2018) and virial radius definition from Bryan & Norman (1998)). The nearest massive galaxy has a stellar mass of $\log M_*/M_\odot = 11.2$ and is at $d = 2273$ pkpc or $\approx 5\times$ its virial radius. The $z = 0.3551$ candidate could be due to an undetected dwarf in principle, but surveys of the CGM/IGM around dwarfs (Johnson et al. 2017) indicate that metal absorption systems are rare beyond the virial radius, and dwarfs are not expected to maintain a hot halo (e.g. Correa et al. 2018).

To determine whether strong O VII systems are expected from the WHIM in isolated environments, we calculated the fraction of predicted strong O VII absorbers as a function of environment using WHIM predictions (Wijers et al. 2019) from the EAGLE cosmological hydrodynamical simulations (Schaye et al. 2015; Crain et al. 2015; McAlpine et al. 2016). We calculated column densities within 2000 km s^{-1} simulation slices and cross-correlated with galaxies as a function stellar mass and projected distance. In total, only $1-3\%$ of the predicted, comparably strong O VII ($\log N(\mathrm{O\,VII})/\mathrm{cm}^{-2} = 15.6$) systems occur in similarly isolated environments ($d > 630$ pkpc to the nearest galaxy of $\log M_*/M_\odot > 9.7$). While the model predictions are subject to non-negligible uncertainties due to treatment of peculiar velocities and feedback, we nevertheless conclude that strong O VII WHIM systems are not expected to be common in isolated environments. Moreover, Bonamente (2018) estimated a 4% probability that the $z = 0.3551$ O VII candidate arises from noise fluctuations.

We conclude that neither of the two candidate O VII absorbers in the spectrum of 1ES 1553+113 are of confident and unbiased intergalactic origin. This implies a 95% upper limit on the number of WHIM O VII absorbers with $W_r \gtrsim 6$ mÅ per unit redshift of $\frac{dN}{dz} < 8$. The lack of strong WHIM X-ray absorption systems suggests that metal enrichment is primarily confined to galaxy halos and their immediate outskirts. This is consistent with the EAGLE simulations which predict that most strong O VII systems arise from metal rich ($> 0.5Z_\odot$) gas at over-densities of $\delta \gtrsim 100$ (see Wijers et al. 2019). Further exploration of the relationship between the WHIM and galaxies requires metallicity independent probes.

4.2. *The origins of broad H I Lyα systems*

While metallicity independent probes of the hot IGM are not currently available (except via stacking), broad H I absorbers ($b > 40$ km s^{-1}) can be used to trace metal poor, warm IGM. While temperature measurements are not possible for most broad H I systems due to lack of detected metals, Savage et al. (2014) found that 78^{+7}_{-12}% of broad H I absorbers with well aligned O VI detections exhibit warm-hot temperatures of $\log T/\mathrm{K} = 5-6$. Danforth et al. (2010) identified 12 broad H I absorbers in the COS spectrum of 1ES 1553+113 at $\Delta v < -10,000$ km s^{-1} from the blazar redshift. None of the broad H I absorbers are coincident with detected galaxies at $d < R_h$. However, all are coincident with at least one luminous galaxy of $L > 0.25L_*$ within $\Delta v = \pm 1000$ km s^{-1} with a median projected distance to the closest one of 700 pkpc. In contrast, narrow ($b < 30$ km s^{-1}; $T < 5 \times 10^4$ K) H I absorption systems detected toward 1ES 1553+113 are further from luminous galaxies on average with a median distance to the nearest one of 1300 pkpc while O VI absorbers are closer to luminous galaxies (350 pkpc; Johnson et al. 2013; Pratt et al. 2018).

4.3. *Summary and conclusions*

Based on deep and highly complete redshift surveys in the field of 1ES 1553+113 we found that:

1. Neither of the two candidate O VII WHIM systems reported toward the sightline (Nicastro et al. 2018)

are of confident and unbiased intergalactic origin. The origins, state, and cosmological mass density of the hot IGM therefore remain uncertain.

2. Low metallicity warm IGM traced by broad H I Lyα absorbers occur $\approx 2\times$ further from luminous ($L > 0.25L_*$) galaxies than O VI absorbers on average, but $2\times$ closer than cool IGM traced by narrow Lyα.

Our findings are consistent with gravitational collapse heating portions of the IGM to form the WHIM. However, they also suggest that feedback is ineffective at enriching the low-z IGM far beyond galaxy/group halos to levels currently observable in UV and X-ray metal ions. Indeed, Liang & Chen (2014) and Johnson et al. (2015) placed upper limits on the mean metallicity of the IGM of $< 0.1Z_\odot$ and pristine ($Z < 0.01Z_\odot$) gas can be found even around massive galaxies (Chen et al. 2019). These observations highlight the need for a variety of WHIM probes coupled with deep galaxy surveys.

ACKNOWLEDGEMENTS

We are grateful to J. Nevalainen, F. Nicastro, and M. Petropoulou for insightful comments. SDJ is supported by a NASA Hubble Fellowship (HST-HF2-51375.001-A). MRD acknowledges support from the Dunlap Institute at the University of Toronto and the Canadian Institute for Advanced Research (CIFAR). J.C.C. acknowledges support by the National Science Foundation under Grant No. AST-1517816. Based on observations from the Magellan, the NOAO Mayall, and NASA/ESA *Hubble* Telescopes. The authors are honored to conduct research on Iolkam Duág (Kitt Peak), a mountain with particular significance to the Tohono Oódham. We made use of the NASA Astrophysics Data System.

Facilities: Magellan, *HST*, Mayall

REFERENCES

Abramowski, A., Aharonian, F., Ait Benkhali, F., et al. 2015, ApJ, 802, 65, doi: 10.1088/0004-637X/802/1/65

Bannister, K. W., Deller, A. T., Phillips, C., et al. 2019, Science, 365, 565. https://arxiv.org/abs/1906.11476

Becker, R. H., White, R. L., & Helfand, D. J. 1995, ApJ, 450, 559, doi: 10.1086/176166

Bonamente, M. 2018, arXiv e-prints. https://arxiv.org/abs/1810.02207

Bryan, G. L., & Norman, M. L. 1998, ApJ, 495, 80, doi: 10.1086/305262

Burchett, J. N., Tripp, T. M., Prochaska, J. X., et al. 2019, ApJL, 877, L20, doi: 10.3847/2041-8213/ab1f7f

Cen, R., & Ostriker, J. P. 1999, ApJ, 514, 1, doi: 10.1086/306949

Chabrier, G. 2003, PASP, 115, 763, doi: 10.1086/376392

Chen, H.-W., & Mulchaey, J. S. 2009, ApJ, 701, 1219, doi: 10.1088/0004-637X/701/2/1219

Chen, H.-W., Johnson, S. D., Straka, L. A., et al. 2019, MNRAS, 484, 431, doi: 10.1093/mnras/sty3513

Connor, T., Zahedy, F. S., Chen, H.-W., et al. 2019, arXiv e-prints, arXiv:1909.10518. https://arxiv.org/abs/1909.10518

Correa, C. A., Schaye, J., Wyithe, J. S. B., et al. 2018, MNRAS, 473, 538, doi: 10.1093/mnras/stx2332

Crain, R. A., Schaye, J., Bower, R. G., et al. 2015, MNRAS, 450, 1937, doi: 10.1093/mnras/stv725

Danforth, C. W., Keeney, B. A., Stocke, J. T., Shull, J. M., & Yao, Y. 2010, ApJ, 720, 976, doi: 10.1088/0004-637X/720/1/976

Danforth, C. W., Keeney, B. A., Tilton, E. M., et al. 2016, ApJ, 817, 111, doi: 10.3847/0004-637X/817/2/111

de Graaff, A., Cai, Y.-C., Heymans, C., & Peacock, J. A. 2019, A&A, 624, A48, doi: 10.1051/0004-6361/201935159

Farina, E. P., Fumagalli, M., Decarli, R., & Fanidakis, N. 2016, MNRAS, 455, 618, doi: 10.1093/mnras/stv2277

Ferland, G. J., Chatzikos, M., Guzmán, F., et al. 2017, RMxAA, 53, 385. https://arxiv.org/abs/1705.10877

Frank, S., Pieri, M. M., Mathur, S., Danforth, C. W., & Shull, J. M. 2018, MNRAS, 476, 1356, doi: 10.1093/mnras/sty294

Green, J. C., Froning, C. S., Osterman, S., et al. 2012, ApJ, 744, 60, doi: 10.1088/0004-637X/744/1/60

Johnson, S. D., Chen, H.-W., & Mulchaey, J. S. 2013, MNRAS, 434, 1765, doi: 10.1093/mnras/stt1137

—. 2015, MNRAS, 449, 3263, doi: 10.1093/mnras/stv553

Johnson, S. D., Chen, H.-W., Mulchaey, J. S., Schaye, J., & Straka, L. A. 2017, ApJL, 850, L10, doi: 10.3847/2041-8213/aa9370

Keeney, B. A., Stocke, J. T., Pratt, C. T., et al. 2018, ApJS, 237, 11, doi: 10.3847/1538-4365/aac727

Khaire, V., & Srianand, R. 2019, MNRAS, 484, 4174, doi: 10.1093/mnras/stz174

Kravtsov, A. V., Vikhlinin, A. A., & Meshcheryakov, A. V. 2018, Astronomy Letters, 44, 8, doi: 10.1134/S1063773717120015

Landoni, M., Falomo, R., Treves, A., & Sbarufatti, B. 2014, A&A, 570, A126, doi: 10.1051/0004-6361/201424232

Liang, C. J., & Chen, H.-W. 2014, MNRAS, 445, 2061, doi: 10.1093/mnras/stu1901

Loveday, J., Norberg, P., Baldry, I. K., et al. 2012, MNRAS, 420, 1239, doi: 10.1111/j.1365-2966.2011.20111.x

McAlpine, S., Helly, J. C., Schaller, M., et al. 2016, Astronomy and Computing, 15, 72, doi: 10.1016/j.ascom.2016.02.004

Mulchaey, J. S., Mushotzky, R. F., Burstein, D., & Davis, D. S. 1996, ApJL, 456, L5, doi: 10.1086/309861

Nelson, D., Kauffmann, G., Pillepich, A., et al. 2018, MNRAS, 477, 450, doi: 10.1093/mnras/sty656

Nevalainen, J., Tempel, E., Ahoranta, J., et al. 2019, A&A, 621, A88, doi: 10.1051/0004-6361/201833109

Nicastro, F., Senatore, F., Gupta, A., et al. 2016, MNRAS, 458, L123, doi: 10.1093/mnrasl/slw022

Nicastro, F., Kaastra, J., Krongold, Y., et al. 2018, Nature, 558, 406, doi: 10.1038/s41586-018-0204-1

Pachat, S., Narayanan, A., Khaire, V., et al. 2017, MNRAS, 471, 792, doi: 10.1093/mnras/stx1435

Pratt, C. T., Stocke, J. T., Keeney, B. A., & Danforth, C. W. 2018, ApJ, 855, 18, doi: 10.3847/1538-4357/aaaaac

Prochaska, J. X., Weiner, B., Chen, H.-W., Cooksey, K. L., & Mulchaey, J. S. 2011, ApJS, 193, 28, doi: 10.1088/0067-0049/193/2/28

Qu, Z., & Bregman, J. N. 2016, ApJ, 832, 189, doi: 10.3847/0004-637X/832/2/189

Rahmati, A., Schaye, J., Crain, R. A., et al. 2016, MNRAS, 459, 310, doi: 10.1093/mnras/stw453

Ravi, V., Catha, M., D'Addario, L., et al. 2019, Nature, 572, 352. https://arxiv.org/abs/1907.01542

Rector, T. A., Gabuzda, D. C., & Stocke, J. T. 2003, AJ, 125, 1060, doi: 10.1086/367802

Rector, T. A., Stocke, J. T., Perlman, E. S., Morris, S. L., & Gioia, I. M. 2000, AJ, 120, 1626, doi: 10.1086/301587

Rovero, A. C., Muriel, H., Donzelli, C., & Pichel, A. 2016, A&A, 589, A92, doi: 10.1051/0004-6361/201527778

Savage, B. D., Kim, T.-S., Wakker, B. P., et al. 2014, ApJS, 212, 8, doi: 10.1088/0067-0049/212/1/8

Schaye, J., Crain, R. A., Bower, R. G., et al. 2015, MNRAS, 446, 521, doi: 10.1093/mnras/stu2058

Shull, J. M., Stevans, M., & Danforth, C. W. 2012, ApJ, 752, 162, doi: 10.1088/0004-637X/752/2/162

Turner, M. L., Schaye, J., Steidel, C. C., Rudie, G. C., & Strom, A. L. 2014, MNRAS, 445, 794, doi: 10.1093/mnras/stu1801

Urry, C. M., Scarpa, R., O'Dowd, M., et al. 2000, ApJ, 532, 816, doi: 10.1086/308616

Wijers, N. A., Schaye, J., Oppenheimer, B. D., Crain, R. A., & Nicastro, F. 2019, MNRAS, 488, 2947. https://arxiv.org/abs/1904.01057

Wurtz, R., Stocke, J. T., Ellingson, E., & Yee, H. K. C. 1997, ApJ, 480, 547, doi: 10.1086/304006